Advances in Analytic Science 2025, 6(1), 2900.
https://doi.org/10.54517/aas2900

Article

Application of ZnO nanoparticles modified with bacterial proteins for the removal of trypan blue effluent

Mai S. Eissa[1,*], Talaat A. Hegajy[2], Elhossein A. Moawed[1]

[1] Chemistry Department, Faculty of Science, Damietta University, Damietta 34517, Egypt
[2] Environmental Science Department, Faculty of Science, Damietta University, Damietta 34517, Egypt
*** Corresponding author:** Mai S. Eissa, essa_mai@yahoo.com

CITATION

Eissa MS, Hegajy TA, Moawed EA. Application of ZnO nanoparticles modified with bacterial proteins for the removal of trypan blue effluent. Advances in Analytic Science. 2025; 6(1): 2900. https://doi.org/10.54517/aas2900

ARTICLE INFO

Received: 3 September 2024
Accepted: 25 December 2024
Available online: 30 May 2025

Abstract: In this study, a bacterial protein-coated nanoparticle system is modified as a new biosorbent. *Escherichia coli* (*E. coli*), and *Staphylococcus aureus* (*S. aureus*) bacterial proteins are collected, and successfully coated onto zinc oxide nanoparticles (ZnONPs). The new biosorbents are combined between the attractive surface properties of the nanoparticles and the adsorbed protein corona. ZnONPs, ZnONPs/*E. coli*, and ZnONPs/*S. aureus* were characterized using X-ray diffraction (XRD), Brunauer-Emmett-Teller (BET), Scanning Electron Microscopy (SEM), and Infrared spectroscopy (FT-IR) studies analysis. The Bradford method was used to ensure the presence of protein corona on the modified surface. The addition of bacterial proteins to the surface of the ZnONPs alters its activity through modifications of its size, shape, surface charge, and other characteristics. The improvement of the functional groups and surface charge of the modified biosorbents makes it more efficient for the removal of dyes. ZnONPs, ZnONPs/*E. coli*, and ZnONPs/*S. aureus* were used for the removal of trypan blue (TB) dye from contaminated wastewater. The TB dye was completely removed (98%–100%) using ZnONPs/*E. coli*, and ZnONPs/*S. aureus* within 25–30 min, whether in the dark or light conditions, over a wide pH range (5–9). The negative values of ΔG showed the spontaneous nature of the removal process. The ΔH values confirmed an endothermic removal in the dark and an exothermic removal in the light. ZnONPs/*E. coli*, and ZnONPs/*S. aureus* were applied for the removal of TB dye from real wastewater samples, and their efficiencies were proven. The average removal rate of TB dye using ZnONPs *E. coli*, and ZnONPs/*S. aureus* was 92 % which is more efficient than that of ZnONPs (87 %), and the average value of RSD% was 1.7 % (n = 5).

Keywords: bacterial proteins; *E. coli*; *S. aureus*; trypan blue dye; ZnONPs

1. Introduction

Water is vital for the survival of all living organisms, and every person needs access to clean water. The textile industries consume a lot of water, and release significant pollutants into the environment [1,2]. The introduction of dyes, from the textile industry, into water alters water transparency due to their toxicity, carcinogenicity, and stability properties [3]. The dye residue disrupts the nutrient balance in marine ecosystems, affecting the human food chain, especially fish [4]. Around 15% of the dyestuffs were lost in industrial effluents during manufacturing processing [5]. Erkurt and Olaifa documented that billions of liters are released as waste yearly in the dyeing process [6]. Dyes undergo chemical changes, and their transformation products may be more toxic and carcinogenic than the dye [7]. Releasing dyes and their breakdown products into the water effluents directly without treatment can cause damage [8].

Synthetic dyes are widely used in many industries, such as textiles, printing, paper, rubber, cosmetics, plastics, and the dying industry [9]. Azo dyes represent the largest and most common synthetic dyes widely used in the textile industry [10]. Azo dyes are characterized by the presence of the azo group (-N=N-) related to aromatic and other function groups such as hydroxyl (-OH), chloro (-Cl), methyl ($-CH_3$), nitro ($-NO_2$), amino ($-NH_3$), carboxyl (-COOH), and sulfonic groups ($-SO_3H$) [11]. Owing to their complex chemical structure, it is hard to decolorize these dyes [12]. TB dye is a diazo anionic dye, in which long exposure; and a high concentration could cause considerable damage to the retina with carcinogenic effects [13].

Different separation techniques have been investigated for dye removal from wastewater. Removal techniques are physical, chemical, and biological, including adsorption, biosorption, coagulation, and oxidation. Biological methods are gaining attention due to their eco-friendly and cost-effective nature, which are the main advantages of the dye removal process [14]. Biosorption processes are concerned with the removal of pollution by using microorganisms and nanotechnology [15]. Biosorbents could be stored for long periods without any opposite effect on their performance, and no metabolic toxin would be released that would affect the public [16].

Various microorganisms can decolorize azo dyes through biosorption or biodegradation, which involves an enzymatic mechanism where bacterial enzymes can cleave the azo bond (-N=N) in azo dyes to form aromatic amine [12]. Using non-viable biomasses has many advantages, such as the fact that there is no need for maintenance or nutrition, and it does not require any activation [16]. Also, non-living or non-growing bacterial biomasses are inexpensive, easy to handle, and have a shorter production time, making them a good alternative to traditional adsorbents. More than 60% of bacterial proteins come from bacterial biomass. Bacterial proteins contain multi-functional groups, including amino acids, which catalyze many chemical reactions [14]. The immobilization of microorganisms onto nano-carriers provides a new technique to obtain biocatalysts for environmental pollution control [17].

Nanoparticles (NPs) have gained significant attention due to their efficiency in the adsorption of water pollutants. Nanoparticles have unique physical and chemical properties, such as surface area, small size, availability, and chemical stability, for being effective sorbents [18]. There is a need to use metal oxide semiconductor nanoparticles for possible biological applications as biomolecules are very sensitive to pH, and temperature [19]. ZnONPs provide a better option for various biological applications due to their easy production, eco-friendly nature, and non-toxic synthesis, [20]. Also, ZnONPs showed significant antibacterial and antifungal activity against many microorganisms [21].

The field of waste treatment has shown considerable interest in immobilizing microbial cells, with reports of their environmental applications [22]. When a nanoparticle enters a biological system, proteins are readily adsorbed on its surface, forming a biological coating called a protein coating, or corona (PC) [23]. The protein corona interacts with the surroundings, instead of the nanoparticles, which determines the nanoparticle's biological impact [24]. Many factors control protein adsorption, such as temperature, pH, ionic strength, and buffer composition, which can be fixed if true physiological conditions are used [25]. Final solid surface coverage is varied and

highly dependent on the individual nature of the protein and the surface. Several examples of protein surface interactions can result in useful functions [26].

This study aims to develop a new biosorbent by surface modification of ZnONPs using bacterial proteins and its applicable use for TB dye removal. The new modified biosorbent combines the biological function of protein corona with the unique properties of ZnONPs. Firstly, ZnONPs were prepared using a well-known precipitation method, and then the bacterial biomasses were collected and coated onto the ZnONPs surface. The physicochemical conditions for removing Trypan Blue (TB) dye, such as pH, initial concentrations, time, and temperature, were investigated under dark and light conditions. Kinetics, isotherm models, and thermodynamic studies were studied.

2. Materials and methods

2.1. Materials

ZnONPs were synthesized by the direct precipitation method, which involves the reduction of zinc sulfate heptahydrate solution using ammonium bicarbonate in the presence of ammonia solution and forming a precursor that undergoes thermal treatment [27]. 15 mL of NH_4OH (7 mol/L, 245 g/L) and 15 mL of $NaHCO_3$ (3 mol/L, 252 g/L) were added to 150 ml of $ZnSO_4 \cdot 7H_2O$ (0.5 mol/L, 144 g/L) dropwise with continuous stirring at room temperature. The product was heated at 60 ℃ for 30 min until a homogeneous and stable colloid solution of zinc carbonate hydroxide was formed. The precipitate was washed with distilled water and ethyl alcohol, filtered triply, and dried at 100 ℃ aerobically for 12 h. ZnONPs were formed by the calcination of the precursor powders at 400 ℃ for 2 h, then ground into fine particles.

E. coli (ATCC25922 NCTC12241), and *S. aureus* (ATCC25923 NCTC129813) were used in this study. Each strain was grown up from a frozen stock by incubation overnight at 37 ℃ on nutrient agar (NA: Oxoid). The bacteria were then inoculated onto nutrient broth (NB: Oxoid) and incubated at 37 ℃ for 24 h. Then the bacterial biomasses were harvested by centrifugation (4 ℃, 15 min, 4000 rpm) and washed twice with sterile Millipore-Q water. Bacterial pellets containing extracellular protein were then suspended in sterile phosphate buffer saline (PBS, pH = 7.2, 10 mM) and diluted to prepare the working culture. Finally, ZnONPs were sonicated with the bacterial proteins at room temperature, filtered, and dried overnight to yield ZnO modified with surface protein.

Bradford reagent was made by dissolving 0.1 g Coomassie Brilliant Blue G-250 in 50 mL of 95% ethanol, then 100 mL of 85% phosphoric acid was added, and the resulting solution was completed to a final volume of 1 liter. A stock solution of trypan blue dye ($C_{34}H_{24}N_6Na_4O_{14}S_4$, 874.88 g/moL, λ_{max} = 598 nm) was prepared by dissolving 0.1 g of dye in 100 mL of distilled water.

2.2. Apparatus

Absorbance measurements were measured on a JASCO (UV-VIS Spectrophotometer, model V-630, Japan). FT-IR spectra were recorded with a JASCO (FT/IR 410 spectrometer, Japan). SEM images were performed with a JEOL (Model

JSM-6510LV, USA). XRD patterns were carried out using an X-ray diffractometer (Brucker, D8 model) using Cu K_α radiation (λ = 1.5418 Å) having a voltage of 40 kV and a current of 40 mA. The samples were scanned in the angular range 2Θ from 10° to 80° with a scanning rate of 0.03° S^{-1}. BET surface area analysis was characterized by nitrogen adsorption-desorption isotherms at 77 ℃ using a NOVA (3200 model, USA). The pH measurements were recorded with a Jenway (3510 model, UK) pH meter. Electrical conductivity was determined using a Keithley Electrical Conductivity with a 6517B electrometer (for resistivity measurements). A magnetic stirrer (Jenway 1000, UK) was used for stirring dye solutions.

2.3. Recommended procedures

The batch experiments were performed to investigate the optimum physico-chemical conditions for the removal of TB dye using ZnONPs, ZnONPs/*E. coli*, and ZnONPs/*S. aureus* under dark and light conditions. The effects of such parameters, including initial dye concentration, contact time, solution pH, and temperature, were studied. 0.1 g of ZnONPs, ZnONPs/*E. coli*, and ZnONPs/*S. aureus* was added to 25 mL of TB dye solutions (known concentration) in 100 mL conical flasks. Then the samples were shaken for the required time, and the remaining dye concentration in the solution after filtration was determined spectrophotometrically. The effect of the presence or absence of light on the dye removal was studied by performing these experiments in the dark and under light.

The percentage of dye removal (%*E*), and adsorption capacity *Q* (mmol/g) of ZnONPs, ZnONPs/*E. coli*, and ZnONPs/*S. aureus* calculated by the following equations:

$$\%E = ((C_0 - C_e)/C_0) \times 100 \quad (1)$$

$$Q = C_o\, E\ V/m \quad (2)$$

where C_o and C_e are the initial and remaining dye concentrations in solution, V is the volume of dye solutions, and m is the mass of the biosorbent.

The surface charge at different pH and pH at zero charge point (pH_{PZC}) of ZnONPs, ZnONPs /*E. coli*, and ZnONPs/S. aureus was evaluated over an initial pH (pH_i) range of 2–14. A 0.5 gm of ZnONPs, ZnONPs/*E. coli*, and ZnONPs/S. aureus was added to 10 mL of each buffer solution and after 24 h, the final pH (pH_f) was also measured. The differences between the initial and final pH values ($\Delta pH = pH_f - pH_i$) were plotted against the initial pH.

The band gap energy (Eg) of ZnONPs ZnONPs/*E. coli*, and ZnONPs/*S. aureus* was determined from UV-Vis measurements using the Tauc equation. For a direct bandgap semiconductor like ZnO [28], the formula used is $(\alpha h\upsilon)^2 = C\,(Eg - h\upsilon)$. Where C is a constant. α is the absorption coefficient ($\alpha = 2.303\ A/t$), where *A* is the absorbance and *t* is the thickness. The energy $h\upsilon$ (in eV) was calculated ($h\upsilon = 1240/\lambda$), where λ is the wavelength in nm. The $(\alpha h\upsilon)^2$ were plotted against $h\upsilon$ and the energy gap can be approximated from the straight portion of the hυ axis at $h\upsilon = 0$.

The total protein concentration adsorbed on ZnO was determined using the Bradford method using bovine serum albumin (BSA) as the protein standard. 0.1 g of

ZnONPs, ZnONPs/*E. coli*, and ZnONPs/*S. aureus* were incubated with the Bradford reagent for 5 min at room temperature, and the absorbance at 595 nm was measured.

The batch experiments were applied on Four different samples from Damietta, Egypt. A 25 mL of samples were spiked with different TB dye concentrations. The samples were shaken with 0.1 g of ZnONPs, ZnONPs/*E. coli*, and ZnONPs/*S. aureus* for 30 min, and the removal rates of TB were examined.

3. Results and discussions

3.1. Characterization of ZnONPs, ZnONPs/*E. coli*, and ZnONPs/*S. aureus*

FT-IR spectra of ZnONPs, ZnONPs/*E. coli*, and ZnONPs/*S. aureus* is shown in **Figure 1**. The absorption peaks of ZnONPs are observed at 3730-2660, 1635, 1508, 1393, 1112, 829, 604, and 446 cm^{-1}. Broadband from 3730 to 2660 cm^{-1}, and peaks at 1639, and 1393 cm^{-1} assigned to the stretching and bending of the hydroxyl group. The characteristic peaks (Zn-O bond) were observed at 829, 604 and 446 cm^{-1}. This result is in good agreement with other works [29–33]. In the spectrum of ZnONPs/*E. coli*, and ZnONPs/*S. aureus*, the broad bands of the hydroxyl group were shifted to 3770-2490 and 3790-2410. Also, the characteristic peaks (Zn-O bond) were shifted to 794, 612 and 438 cm^{-1} and new peaks were observed at 3507, 1671, 990 and 676 cm^{-1}. The peaks at 3507 and 1671 cm^{-1} are assigned to the stretching of N-H and C=O of microbial protein, while the peaks at 990 and 676 cm^{-1} represent the bonding between the microbial protein function group and Zn^{2+} of ZnO. The microbial proteins were successfully immobilized on the surface of ZnONPs.

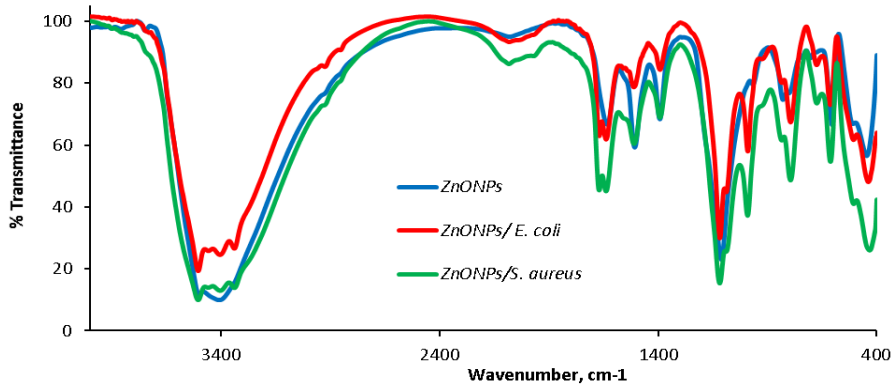

Figure 1. Infrared spectra of ZnONPs, ZnONPs/*E. coli*, and ZnONPs/*S. aureus*.

The UV-Vis absorption spectra of ZnONPs, ZnONPs/*E. coli*, and ZnONPs/*S. aureus* was carried out in the solid state using the Nujol mulls method (**Figure 2**). The absorption spectrum of ZnONPs depends on several parameters, such as route of preparation, temperature, size, and shape [34,35]. The specific absorption peaks of ZnONPs were observed at 201, 203, 208–211, 216, 222–226, 236, 238–271, 273–275 and 278–381 nm. The band position at 278-381 nm confirmed the formation of nanoparticles. In the spectra of ZnONPs/*E. coli*, and ZnONPs/*S. aureus*, the characteristic band of nanoparticles was shifted to 278–374 and 278–340 nm, respectively.

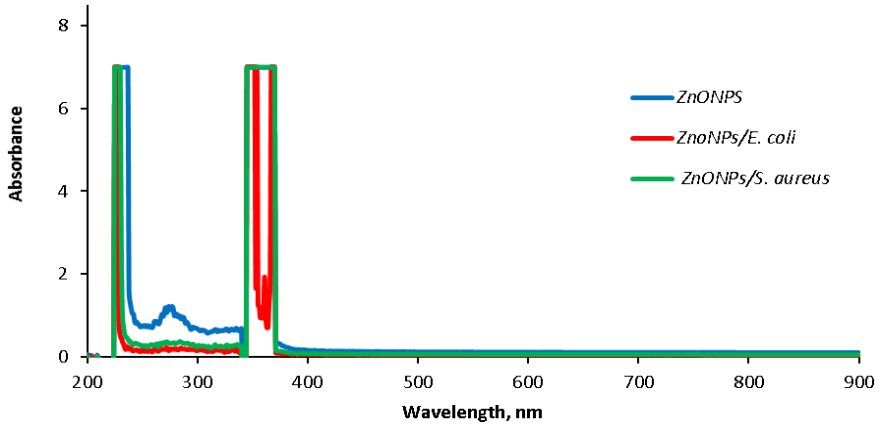

Figure 2. UV spectra of ZnONPs, ZnONPs/*E. coli*, and ZnONPs/*S. aureus.*

Eg of ZnONPs, ZnONPs/*E. coli*, and ZnONPs/*S. aureus* was estimated by plotting the graph of $(\alpha hv)^2$ and hυ as exhibited in **Figure 3**. The approximated values were achieved by extrapolating the straight portion to the *hv* axis at $(\alpha hv) = 0$. The energy gap of ZnONPs, ZnONPs/*E. coli*, and ZnONPs/*S. aureus* was estimated to be 3.24, 3.2, and 3.16 eV, respectively.

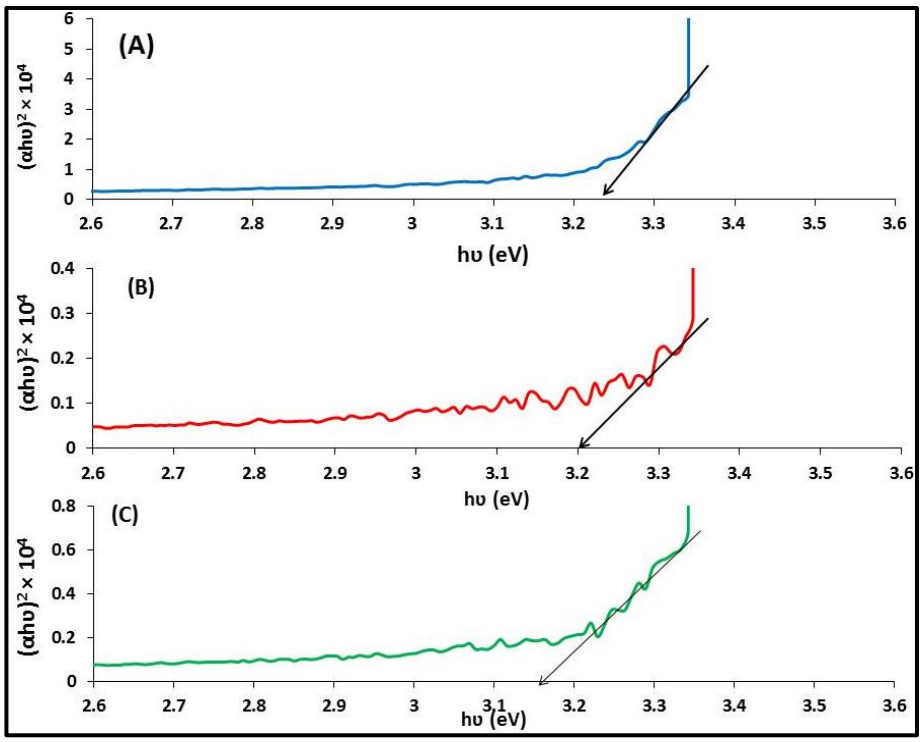

Figure 3. Band gap energies: **(A)** ZnONPs; **(B)** ZnONPs/*E. coli*; **(C)** ZnONPs/*S. aureus*.

Electrical conductivity (σ) values of ZnONPs, ZnONPs/*E. coli*, and ZnONPs/*S. aureus* were found 6.1×10^{-7}, 10.2×10^{-7}, and 28.4×10^{-7} Ω^{-1} m^{-1} in the solid state. The result showed an improvement in the polarity of ZnONPs/*E. coli*, and ZnONPs/*S. aureus* when compared to that of ZnONPs. The results confirmed that the lower the energy gap, the higher the conductivity.

The pH of zero-point charge (pH_{PZC}) is an important characteristic of a sorbent as it helps in determining the pH value at which the surface of the sorbent becomes electrically neutral and facilitates in predicting the surface behavior of sorbents over a wide pH range. The difference between the initial and final pH values ($\Delta pH = pH_f - pH_i$) was plotted as a function of the pH_i and the pH_{PZC} was the pH at which the initial pH equals the final pH. The pH_{ZPC} value of ZnONPs, ZnONPs/*E. coli*, and ZnONPs/*S. aureus* were 7.1, 7.3, and 7.2 (**Figure 4**). At pH lower than the pH_{PZC}, the surfaces of sorbents would be positively charged, and negatively charged at pH higher than pH_{PZC}. The maximum values of ΔpH for ZnONPs, ZnONPs/*E. coli*, and ZnONPs/*S. aureus* were +2.97, +3.37, +3.41 at pH 3 and −1.8, −1.89, and −2 at pH 9. The net surface charge of ZnONPs/*E. coli*, and ZnONPs/*S. aureus* was higher than that of the ZnONPs. The net surface charges of the modified ZnONPs/*E. coli*, and ZnONPs/*S. aureus* were improved, explaining the increase in electrical conductivity.

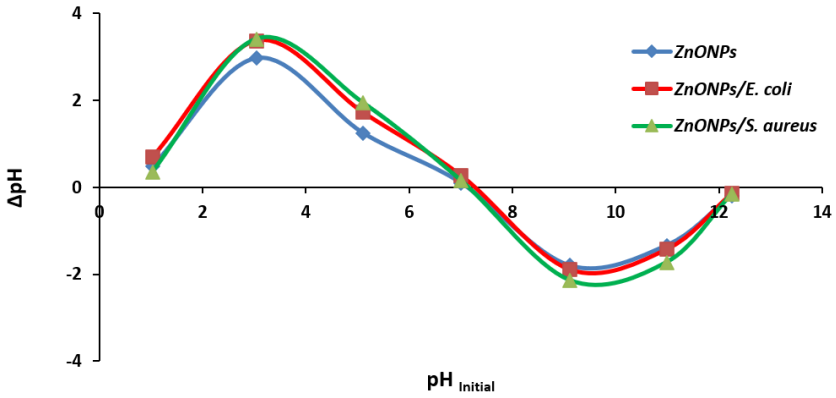

Figure 4. pH_{ZPC} of ZnONPs, ZnONPs/*E. coli*, and ZnONPs/*S. aureus.*

The X-ray diffraction spectra of ZnONPs, ZnONPs/*E. coli*, and ZnONPs/*S. aureus* were displayed (**Figure 5**). The characteristic diffraction patterns of ZnONPs at 2Θ = 31.78°, 32.73°, 34.36°, 36.17°, 47.54°, 56.54°, 62.77°, and 67.83°. The XRD pattern ZnONPs exhibits a monoclinic crystal system (space group C2/C) with lattice parameters of a = 13.47 Å, b = 18.82 Å, c = 10.39 Å, $\alpha = \gamma = 90°$ and β =106.43°. While the characteristic diffraction patterns of ZnONPs/*E. coli* were shifted to 2Θ = 31.77°, 32.83°, 34.45°, 36.25°, 47.69°, 56.59°, 62.87°, and 67.20°. The ZnONPs/*E. coli* X-ray pattern exhibits a monoclinic crystal system (space group P21/N) with lattice parameters of a = 12.43 Å, b = 4.52 Å, c = 11.44 Å, $\alpha = \gamma = 90°$, and β = 106.91°. The characteristic diffraction patterns of ZnONPs/*S. aureus* were shifted to 2Θ = 31.74°, 32.74°, 34.39°, 36.22°, 47.65°, 56.53°, 62.79°, and 67.93°. X-ray pattern of ZnONPs/*S. aureus* exhibit an orthorhombic crystal system (space group CCCA) with lattice parameters of a = 19.93 Å, b = 18.87 Å, c = 13.1 Å, and $\alpha = \beta = \gamma = 90°$. The results showed that modification of ZnONPs with bacterial proteins caused a phase change in the crystal structure.

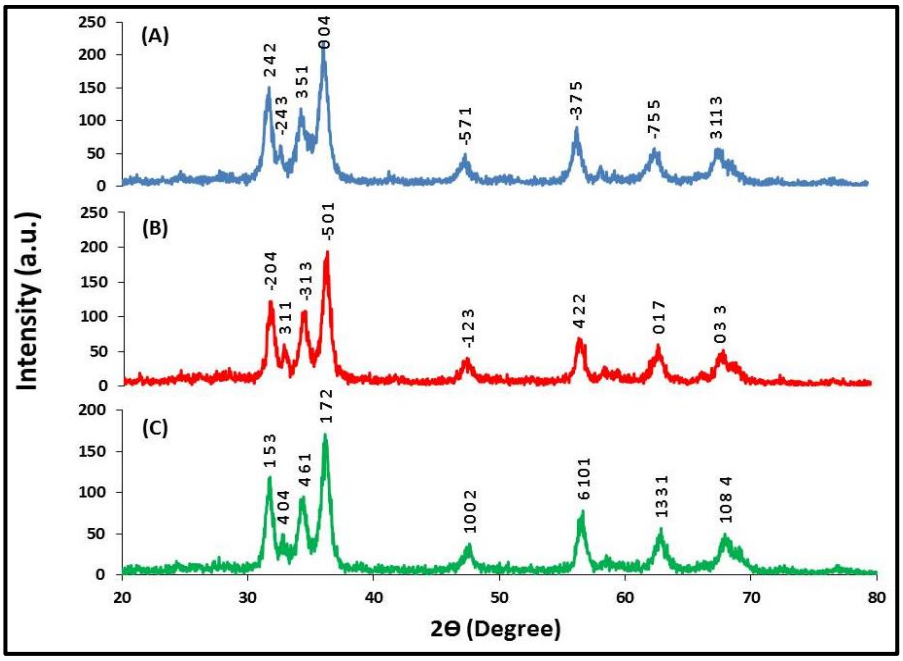

Figure 5. XRD patterns: **(A)** ZnONPs; **(B)** ZnONPs/*E. coli*; **(C)** ZnONPs/*S. aureus*.

The particle size of ZnONPs, ZnONPs/*E. coli*, and ZnONPs/*S. aureus* was calculated using the Scherer equation: $\tau = K\,\lambda/\beta\,\cos\Theta$ Where τ is the mean crystalline size, *K* equals 0.97, λ is the X-ray wavelength (0.15418 nm), β is the peak full width at half maximum (FWHM) in radians, and θ is the Bragg diffraction angle. The decrease in FWHM, with modifications to particle size, led to sharper diffraction peaks, and these strong and narrow diffraction peaks indicated that the nanoparticles have good crystallinity and size [34]. The average sizes of ZnONPs, ZnONPs/*E. coli*, and ZnONPs/*S. aureus* were found to be 18.4, 27.2, and 28.7 nm. Such an increase in size, approximately 9–10 nm thick layers, confirms the protein coating on the surface of ZnONPs.

BET surface area analysis and Barrett-Joyner-Halenda (BJH) pore size and volume analysis were estimated by N_2 adsorption-desorption isotherms. ZnONPs, ZnONPs/*E. coli*, and ZnONPs/*S. aureus* adsorption isotherms (**Figure 6**) match a type-IV curve, which is expressive for porous materials. The average values of pore radius for ZnONPs, ZnONPs/*E. coli*, and ZnONPs/*S. aureus* are 3.9–45, 3.8–28 and 3.6–30 nm. The surface area of ZnONPs, ZnONPs/*E. coli*, and ZnONPs/*S. aureus* are 31.5, 27.9, and 39.9 m^2/g. The surface area of ZnONPs/*E. coli* decreases generally because of pore blocking after protein adsorption. While ZnONPs/*S. aureus* shows a higher surface area because the pores are too wide or the phase change (XRD patterns) creates more heterogeneity and roughness. The pore volumes of ZnONPs, ZnONPs/*E. coli*, and ZnONPs/*S. aureus* are 14.7×10^{-2}, 15.7×10^{-2} and 23.5×10^{-2} cm^3/g at P/Po 0.985. The ratio of mesopore to micropore volumes of ZnONPs (13.5×10^{-2}: 12×10^{-2} cm^3/g) is 11:1. While the ratio of ZnONPs/*E. coli* (14.5×10^{-2}: 11.6×10^{-2} cm^3/g) is 12:1 and the ratio of ZnONPs/*S. aureus* (21.96×10^{-2}: 15.4×10^{-2} cm^3/g) is 14:1; such ratios would be a good indicator for effective removal of dyes.

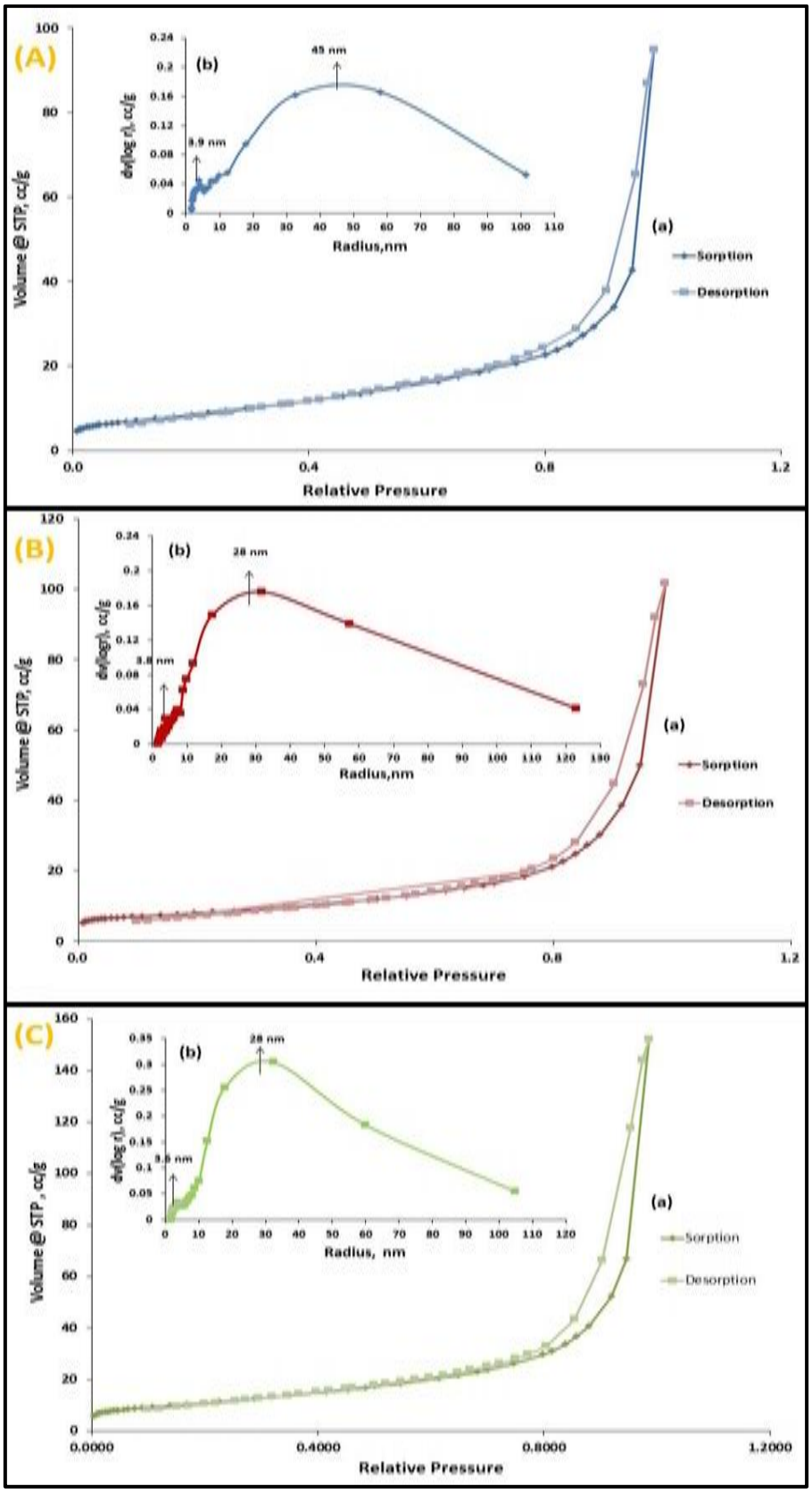

Figure 6. BET curves for the sorption and desorption of N_2 gas onto: **(A)** ZnONPs; **(B)** ZnONPs/*E. coli*; **(C)** ZnONPs/*S. aureus*.

The amount of bound protein adsorbed on ZnONPs can be quantified using the Bradford assay. The assay is based on the observation that the λ_{max} for an acidic solution of Coomassie Brilliant Blue G-250 shifts from 465 nm to 595 nm when binding to proteins. The formation of a protein-dye complex stabilizes the blue form of the Coomassie dye, and the amount of complex formed is a measure for amino acid residues [36]. Thus, the amount of extracellular protein successfully adsorbed on the surface of ZnONPs/*E. coli*, and ZnONPs/*S. aureus* can be monitored. While ZnONPs showed the absence of detectable protein content, ZnONPs/*E. coli*, and ZnONPs/*S. aureus* showed a significant value of absorbance at 595 nm, implying the presence of protein content on the new modified biosorbent. This increase in absorbance at 595 nm is proportional to the amount of the bound dye, and the amount of protein present. The results showed that approximately 3.3 and 1.7 µg proteins were adsorbed on 0.1 g of ZnONPs/*E. coli*, and ZnONPs/*S. aureus*.

The SEM images of ZnONPs, ZnONPs/*E. coli*, and ZnONPs/*S. aureus* were taken at magnifications of 1000, 5000, 10,000, and 20,000 x. The SEM image of ZnONPs shows a spherical-like morphology, while the coverage of bacterial protein on the surface of ZnONPs/*E. coli*, and ZnONPs/*S. aureus* may conceal this shape (**Figure 7**). SEM images ZnONPs/*E. coli*, and ZnONPs/*S. aureus* have a rough surface containing many spaces, and pores while ZnONPs are much smoother. In addition, agglomeration was shown with small particles. ZnONPs/*E. coli* shows better coverage of its protein on its surface and has fewer spaces. ZnONPs/*S. aureus* shows lower coverage but more spaces and pores. Which indicate that ZnONPs/*E. coli*, and ZnONPs/*S. aureus* have good sorption characteristics.

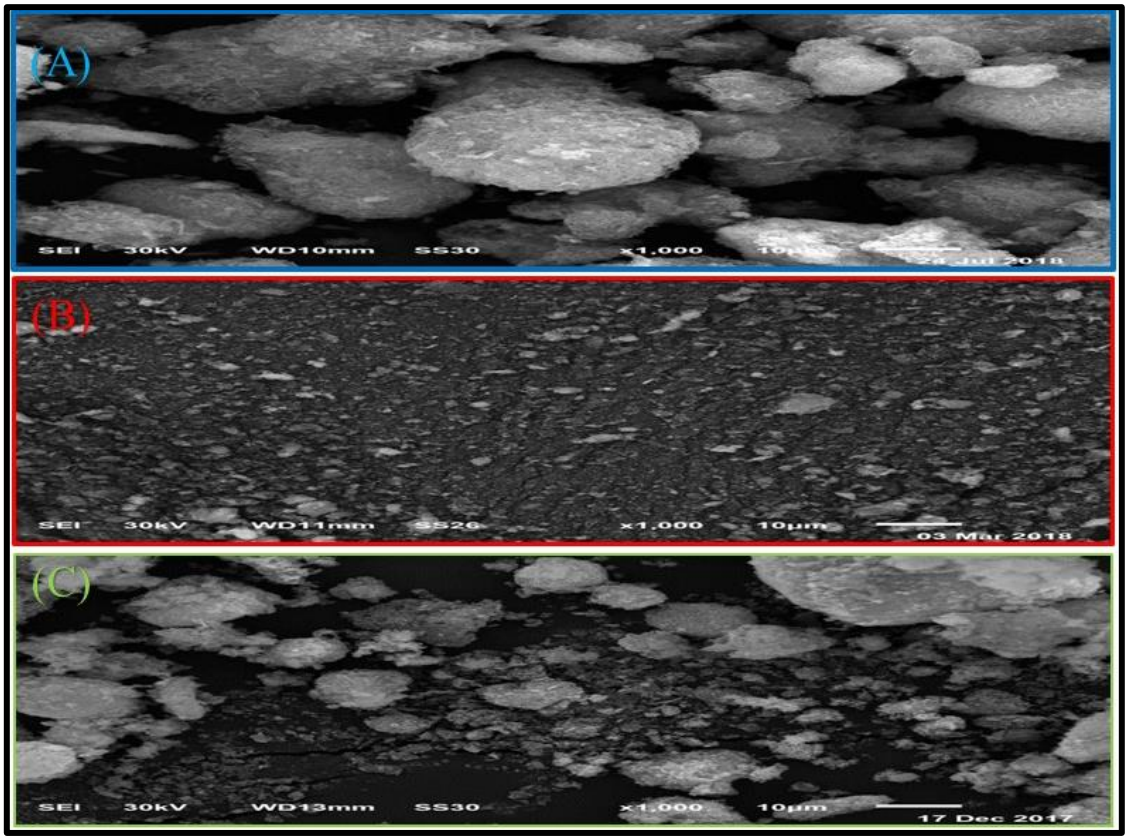

Figure 7. SEM at magnifications of 1000X: **(A)** ZnONPs; **(B)** ZnONPs/*E. coli*; **(C)** ZnONPs/*S. aureus*.

3.2. Optimum conditions for TB dye removal

3.2.1. Effect of pH

The removal of TB dye using ZnONPs, ZnONPs/*E. coli*, and ZnONPs/*S. aureus* was studied at different pH values (1–13) under dark/light conditions. The removal percentages of TB dye were plotted against the initial pH value (**Figure 8**). The maximum removal percentage of TB dye using ZnONPs, ZnONPs/*E. coli*, and ZnONPs/*S. aureus* was achieved at pH range 3–9, whether in the dark or light. The removal rates of TB using ZnONPs were decreased from 93% to 88% in the dark, and from 87% to 86% in the light at pH range 3–9. While the removal rates of TB using ZnONPs/*E. coli* increased from 99% to 100% in the dark, and from 96% to 98% in the light. And the removal rates of TB using ZnONPs/*S. aureus* increased from 97% to 99% in the dark, and from 95% to 96% in light. The results showed higher removal rates of TB using ZnONPs/*E. coli*, and ZnONPs/*S. aureus* compared to ZnONPs in the dark and light.

ZnONPs is an amphoteric oxide, which can react with both H^+ and OH^- ions due to hydroxide coating on its surface. The functional groups of the bacterial proteins behave in terms of acid-base chemistry as a response to variable pH conditions [37]. In an acidic medium, the sorbent surface is positively charged (attracting TB anionic dye). Conversely, the surface is negatively charged (repelling TB anionic dye) in an alkaline medium. In addition, the spaces and pores on the surfaces of ZnONPs/*E. coli*, and ZnONPs/*S. aureus*, as shown in SEM images and BET results, is improving its sorption characteristic compared to ZnONPs.

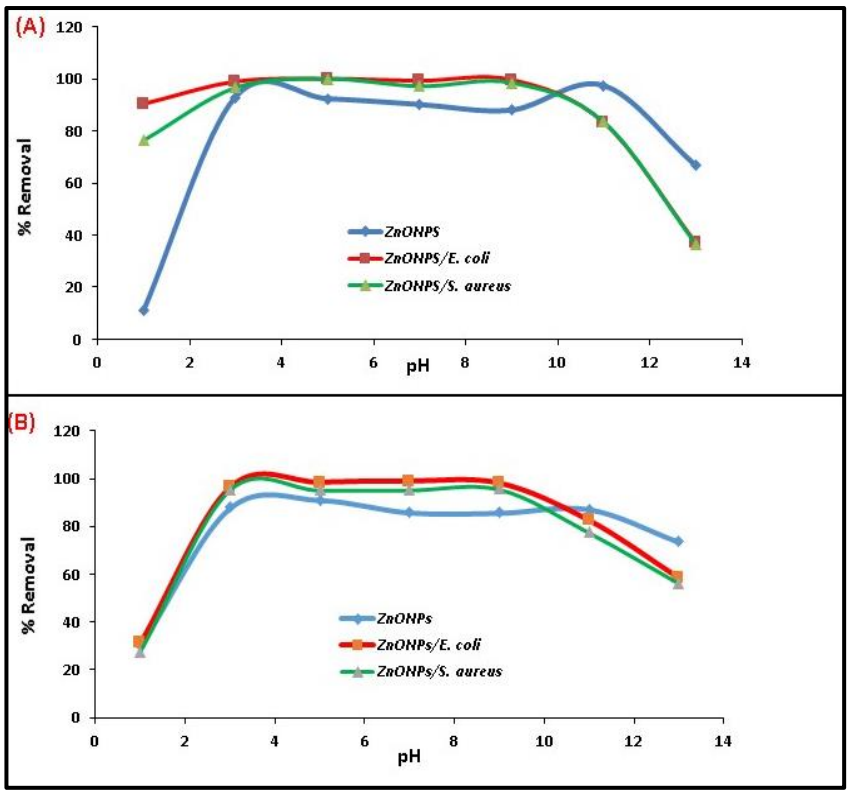

Figure 8. Effect of initial pH on the removal of TB using ZnONPs, ZnONPs/*E. coli*, and ZnONPs/*S. aureus* under: **(A)** dark condition; **(B)** light condition.

3.2.2. Thermodynamic behavior

The effect of temperature on the removal of TB dye using ZnONPs, ZnONPs/*E. coli*, and ZnONPs/*S. aureus* under dark/ light condition was studied. The removal efficiency of TB dye was investigated at temperature range 25–62 ℃ and their removal rates were plotted against the solution temperature (**Figure 9**).

Under dark conditions, the removal rates of TB using ZnONPs were decreased from 76% to 62% with increasing temperature range (from 25 to 62 ℃). While the removal rates of TB dye using ZnONPs/*E. coli*, and ZnONPs/*S. aureus* were increased from 78, and 80% to 98, and 97%. This increase can be explained in terms of destroying the TB self-aggregation and increasing the TB monomer concentration. This small monomer binds surface bacterial protein easier than the self-aggregate because of the lighter weight [38]. The absence of microbial proteins on the ZnONPs surface make it not affected with this property and the removal rates decreased with increasing temperature.

While under light conditions, the removal rates of TB dye using ZnONPs, ZnONPs/*E. coli*, and ZnONPs/*S. aureus* were decreased from 85%, 88%, and 84% to 81%, 66%, and 71% with increasing temperature (from 25 to 58 ℃). These results showed that temperature has a reverse effect on the efficiency of the removal of TB under light while it approximately has not affected on ZnONPs. These results make the removal of TB dye using ZnONPs/*E. coli*, and ZnONPs/*S. aureus* from hot wastewater industries is more efficient under darker conditions than in the presence of light.

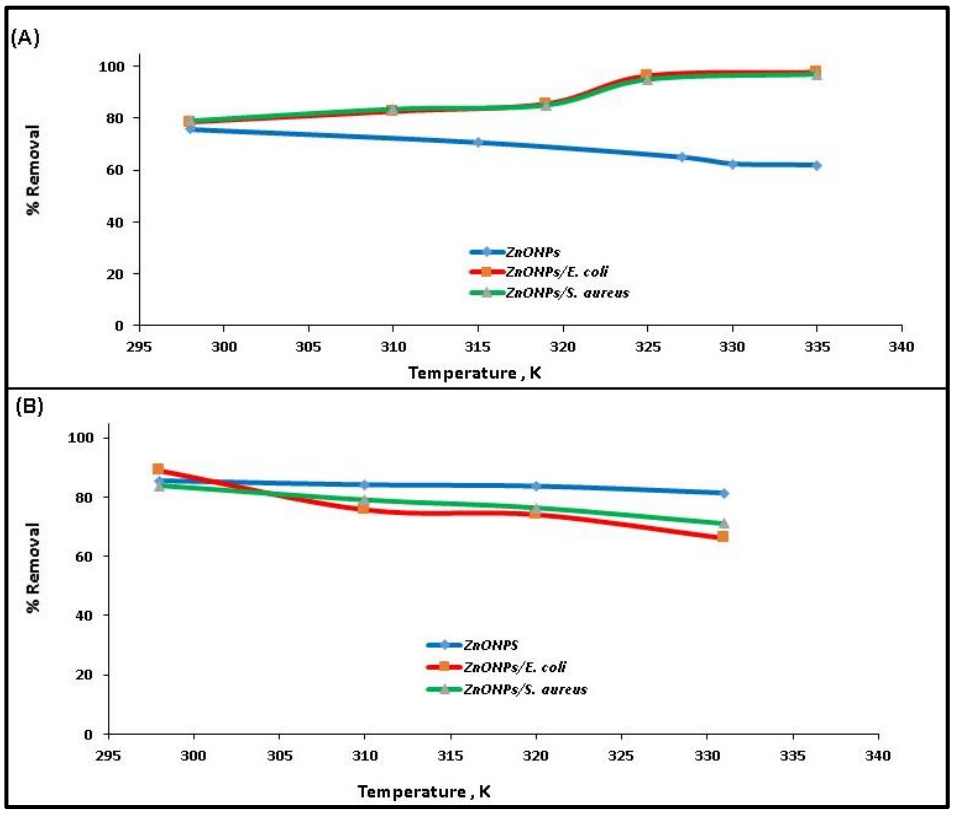

Figure 9. Effect of temperature on the removal of TB using ZnONPs, ZnONPs/*E. coli*, and ZnONPs/*S. aureus* under: **(A)** dark condition; **(B)** light condition.

The thermodynamic parameters such as Gibbs free energy change (ΔG), enthalpy (ΔH), and entropy (ΔS) were calculated using the following equations:

$$\mathrm{Ln}\, K = -\Delta H/RT + \Delta S/R \quad (3)$$

$$\Delta G = \Delta H - T\Delta S \quad (4)$$

where *K* is the equilibrium constant for sorption, *R* is the gas constant (8.314 J/mol K) and *T* is the temperature (K). Equilibrium constant *K* can be calculated using the following equation: $K = C_a/C_e$, where C_a is the equilibrium dye concentration on the sorbent, C_e is the equilibrium dye concentration in the solution (mg/ L). Plots of Ln (K) versus 1/T are linear with an average R^2 of 0.873 and 0.944 and the values of ΔH and ΔS can be determined from the slope and intercept then (ΔG) was calculated.

The average values of ΔG were between −2.56 and −4.42 kJ/mol for TB dye under dark and light conditions (**Table 1**). The negative sign of ΔG is due to the spontaneous nature of the removal process. The ΔG values were between −20 and 0 kJ/mol which indicated that physical forces dominate the removal mechanism [21]. ΔG in light is approximately twice that in darkness and this increase in negative values of ΔG indicates that the removal is more favorable in light conditions. Under dark conditions, the decrease in negative values of ΔG for ZnONPs with increasing temperature indicates that the removal process is more favorable at low temperature. The increase in negative values of ΔG for ZnONPs/*E. coli*, and ZnONPs/*S. aureus* by a similar temperature increase indicates that the removal is more favorable at higher temperature. While under light conditions, ΔG for ZnONPs, ZnONPs/*E. coli*, and ZnONPs/*S. aureus* are all decreased with increasing temperature, implying that removals are favorable at low temperature in the presence of light [39].

The average values of ΔH for the removal of TB dye using ZnONPs/*E. coil*, and ZnONPs/*S. aureus* were 54.6 and −25.5 kJ/mol in the dark and under light (**Table 1**). The positive ΔH value reveals an endothermic removal process in the dark while the negative ΔH value confirms an exothermic removal process in the presence of light. Also, the values of ΔH for ZnONPs were −15.41 and −6.95 kJ/mol which confirms the exothermic nature of the removal of TB dye using ZnONPs whether in the darkness or in the light.

The average values of ΔS for TB dye using ZnONPs/*E. coli*, and ZnONPs/*S. aureus* were 0.19 and −0.07 kJ/mol.K, under dark and light conditions (**Table 1**). The positive value of ΔS indicates the increasing of the entropy during the removal process in the dark. While the negative value suggests that TB dye concentration increases on its surface which leads to a decrease in randomness during the removal process in the light. The values of ΔS for ZnONPs were −0.04 and −0.008 kJ/mol in dark/light. This decrease in entropy reveals the favorability of the removal process in the dark/light condition.

Table 1. Thermodynamic parameters for removing TB dye under dark/light conditions.

Sorbent	ΔH (kJ/mol)	ΔS (kJ/mol.K)	ΔG (kJ/mol)	R^2
Dark				
ZnONPs	−15.41	−0.04	−2.87	0.979
ZnONPs/*E. coli*	60.66	0.21	−2.24	0.813
ZnONPs/*S. aureus*	48.54	0.17	−2.58	0.827
Light				
ZnONPs	−6.95	−0.008	−4.41	0.937
ZnONPs/*E. coli*	−33.16	−0.095	−4.79	0.903
ZnONPs/*S. aureus*	−17.86	−0.046	−4.05	0.992

3.2.3. Sorption isotherms

The effect of initial TB concentrations (4.5–27.5 µmol/L, 4–24 mg/L) on removal capacities (Q_C) of ZnONPs, ZnONPs/*E. coli*, and ZnONPs/*S. aureus* were investigated under dark/light conditions. The removal capacities were plotted with initial dye concentration with an average R^2 of 0.997 and zero intercept (0.0001, **Figure 10**). The removal capacity (Q_C) increased with the sequential increase in initial dye concentrations. The removal capacities of ZnONPs/*E. coli*, and ZnONPs/*S. aureus* for TB dye are 7.5 and 7.7 µmol/g (6.6 and 6.8 mg/g) under dark conditions. These values indicated a better removal capacity compared to ZnONPs (7.2 µmol/g, 6.3 mg/g) as shown in **Table 2**. Under light conditions, the removal capacities of ZnONPs/*E. coli*, and ZnONPs/*S. aureus* for TB dye are 6.5 and 6.6 µmol/g (5.7 and 5.72 mg/g). These values indicated better removal capacity when compared to that of ZnONPs (7µmol/g, 15.6 mg/g).

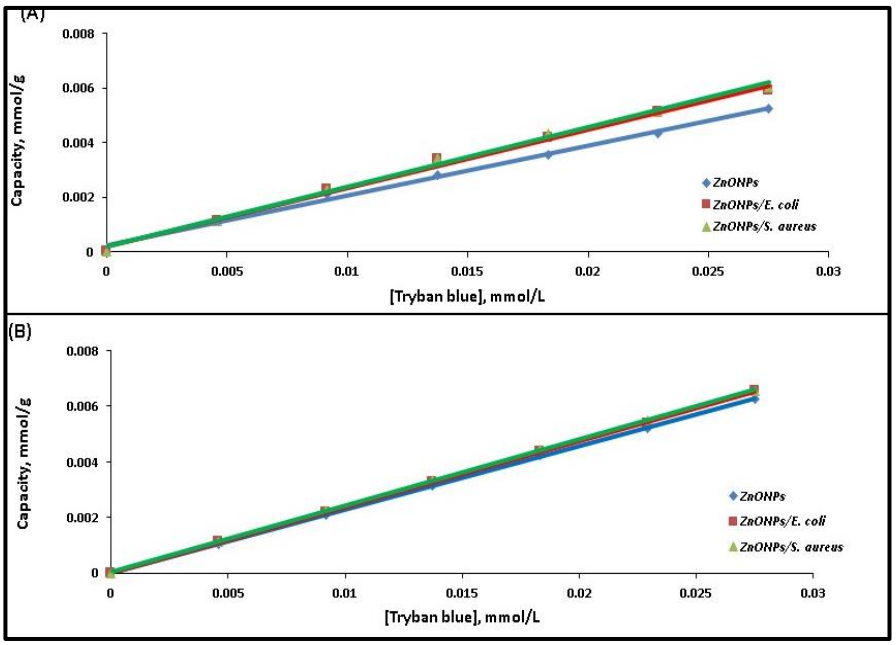

Figure 10. Effect of initial concentration on the removal of TB using ZnONPs, ZnONPs/*E. coli*, and ZnONPs/*S. aureus* under: **(A)** dark condition; **(B)** light condition.

The removal rate of TB using ZnONPs, ZnONPs/*E. coli*, and ZnONPs/*S. aureus* decreased from 99, 100, and 100 % to 76, 86, and 88 %, with increasing TB concentrations (from 4 to 24 mg/L) in the dark. Also, the removal rate of TB using ZnONPs, ZnONPs/*E. coli*, and ZnONPs/*S. aureus* decreased, with increasing TB concentrations (from 4 to 24 mg/L), from 93%, 97%, and 99 % to 91%, 95%, and 95%, when exposed to light.

The experimental data were analyzed using Langmuir (5), Freundlich (6), Dubinin-Radushkevich (7) and Temkin (8).

$$C_e/Q_c = (1/K_L b) + (C_e/K_L) \quad (5)$$

$$\text{Log}\, Q_c = \text{Log}\, K_F + 1/n\ \text{Log}\, C_e \quad (6)$$

$$\text{Ln}\, Q_c = \text{Ln}\, K_{D-R} - \beta\varepsilon^2 \quad (7)$$

$$Q_c = B\ \ln A + B\ \ln C_e \quad (8)$$

where Q_c (mmol/g) is the dye adsorbed at equilibrium and C_e (mmol/ L) is the dye concentration at equilibrium. Langmuir constants K_L (mmol/ g) and b (L/ mmol) are related to removal capacity and removal rate. K_F and n are Freundlich constants related to removal capacity and removal intensity. $K_{D\text{-}R}$ is the maximum dye amount retained onto the sorbent, β (mol^2/ kJ^2) is Dubinin-Radushkevich constant and ε (J/mol) is Polanyi potential. B and A are Temkin constants related to the heat of sorption and max binding energy. $B = RT/b$ where R is the gas constant (8.314 J/mol K), T is the temperature (K), and b is Temkin isotherm constant.

Table 2. Characteristic of equilibrium curves for removing TB dye under dark/light conditions.

Sorbent	***Q* (mg/g)**	**R^2**	**Intercept**
Dark			
ZnONPs	6.32	0.994	0.00022
ZnONPs/*E. coli*	6.56	0.995	0.00019
ZnONPs/*S. aureus*	6.75	0.995	0.00018
Light			
ZnONPs	5.46	0.999	0.000009
ZnONPs/*E. coli*	5.7	0.999	0.000015
ZnONPs/*S. aureus*	5.72	0.999	0.000037

The plot of C_e/Q_c against C_e according to the Langmuir model gives a linear relationship with R^2 values of 0.951 and 0.685 for Dark and light (**Table 3**). $R_L = 1/(1 + bC_0)$, where C_0 is the highest initial concentration of dye, was used to investigate the favorability of the removal of TB dye. The values of R_L are 0.022 and 0.14 ($0 < R_L < 1$) for dark and light indicating the removal of TB dye was favorable. The high R^2 of ZnONPs/*E. coli*, and ZnONPs/*S. aureus* in the dark assumes that TB dye molecules can be adsorbed at certain sites, the functional groups on the modified surface.

The relation between log Q_c versus log C_e was linear with R^2 values of 0.938, and 0.989 for Dark and light (**Table 3**). The Freundlich constants ($1/n < 1$) are 0.2, and 0.76 for Dark and light, which may be due to the heterogeneous surface of ZnONPs/*E. coli*, and ZnONPs/*S. aureus* with a non-uniform heat distribution over the surface. The values of n are 5.1, and 1.4 for Dark and light, indicating that the sorption is favorable. Freundlich model can be described as the sorption equation considering a heterogeneous surface and multilayer adsorption to the binding sites located on the surface of the sorbent.

Table 3. Comparison of Langmuir and Freundlich parameters for removing TB dye under dark/light conditions.

	Langmuir		**Freundlich**	
Sorbent	R^2	R_L	R^2	$1/n$
Dark				
ZnONPs	0.898	0.04	0.923	0.23
ZnONPs/*E. coli*	0.974	0.02	0.943	0.21
ZnONPs/*S. aureus*	0.982	0.005	0.949	0.16
Light				
ZnONPs	0.401	0.33	0.992	0.91
ZnONPs/*E. coli*	0.726	0.07	0.985	0.84
ZnONPs/*S. aureus*	0.929	0.02	0.991	0.54

The plots of ln Q_c versus ε^2 are found to be linear with good R^2 values of 0.929 and 0.974 and β values are −0.010 and −0.011 kJ^2/mol^2 for dark and light (**Table 4**). The sorption energy (ΔE) was estimated using the following equation: $E = 1/\sqrt{-2\beta}$, the result showed that average values of ΔE are 7 and 6.7 kJ/ mol (< 8 kJ/mol), which suggests a physical sorption in the dark or in the light.

The plots of Q against lnC_e give a linear relationship with a correlation coefficient (R^2 = 0.901 and 0.909) for dark and light (**Table 4**). The average b values are 3808 and 984 kJ/mol for dark and light which are higher than 80 kJ/mol, referring to chemical sorption.

Table 4. Comparison of Temkin and Dubinin-Radushkevich parameters for removing TB dye under dark/light conditions.

Sorbent	**Temkin**		**Dubinin–Radushkevich**		
	R^2	b (kJ/mol)	R^2	β (kJ^2/mol^2)	ΔE (kJ/mol)
Dark					
ZnONPs	0.838	4288	0.893	−0.01	7.06
ZnONPs/*E. coli*	0.928	3062	0.943	−0.0108	6.81
ZnONPs/*S. aureus*	0.936	4073	0.952	−0.0098	7.15
Light					
ZnONPs	0.916	953	0.957	−0.0116	6.56
ZnONPs/*E. coli*	0.882	760	0.977	−0.0114	6.62
ZnONPs/*S. aureus*	0.929	1239	0.989	−0.0105	6.91

3.2.4. Sorption kinetics

The effect of contact time on the removal of TB dye using ZnONPs, ZnONPs/*E. coli*, and ZnONPs/*S. aureus* was investigated under dark and light conditions. The time required for 98%–100 % removal of TB dye using ZnONPs/*E. coli*, and ZnONPs/*S. aureus* is 25–30 min (**Figure 11**). The removal rates of dyes were initially fast, where about 81 % of the total TB dyes were removed at the first 1m, and then the rate became slower as the time increased (19 %) were removed since 24–29 min). This rapid removal rate of TB dye is mainly because of vacant sorption sites which could adsorb more dye molecules [21].

The removal rates of TB using ZnONPs, ZnONPs/*E. coli*, and ZnONPs/*S. aureus* at 1 min were 76%, 79% and 80% (dark) and 76%, 80%, 81% (light). The removal rates of TB using ZnONPs reached 98% (dark) and 91% (light) after 60 min., while the removal rates of TB using ZnONPs/*E. coli*, and ZnONPs/*S. aureus* reached 100% (dark), and 99% (light) after 25, and 30 min. The removal rates of dyes using ZnONPs/*E. coli*, and ZnONPs/*S. aureus* is higher than that of ZnONPs. The high removal rates of ZnONPs/*E. coli*, and ZnONPs/*S. aureus* may be due to the porosity of its surfaces as it appeared in SEM image. The porosity is a measure of void spaces and pores within a material which Leads to enhancing the ZnONPs/*E. coli*, and ZnONPs/*S. aureus* sorption performance.

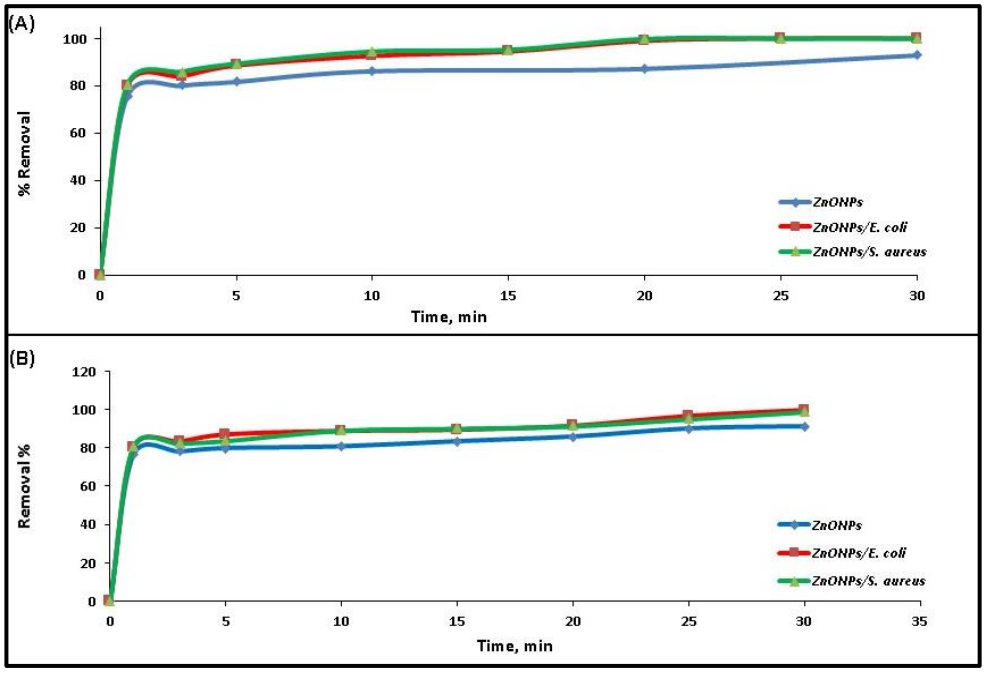

Figure 11. Effect of stirring time on the removal of TB dye using ZnONPs, ZnONPs/*E. coli*, and ZnONPs/*S. aureus* under: **(A)** dark condition; **(B)** light condition.

The experimental data for the removal of TB on ZnONPs, ZnONPs/*E. coli*, and ZnONPs/*S. aureus* were analyzed using pseudo first order kinetic (9) and pseudo second order kinetic models (10).

$$log\ Q_e - Q_t = log\ Q_e - (K_1 t/2.303) \quad (9)$$

$$t/Q_t = \left(1/K_2 {Q_e}^2\right) + t/Q_e \quad (10)$$

where Q_e (mmol/ g) is the sorption capacity at equilibrium and Q_t (mmol/ g) is the sorption capacity at time *t*. K_1 (min^{-1}) is the pseudo first rate constant, and K_2 (g/ mmol min) is the pseudo second order rate constant.

Table 5. Comparison of kinetic parameters for removing TB dye under dark/light conditions.

Sorbent	Pseudo first order			Pseudo second order		
	R^2	K_1 (min^{-1})	$t_{1/2}$ (min)	R^2	K_2 (g/mmol min)	$t_{1/2}$ (min)
	Dark					
ZnONPs	0.9585	0.04	14.84	0.9988	434.52	1.08
ZnONPS/*E. coli*	0.9681	0.14	4.86	0.9993	622.44	0.69
ZnONPs/*S. aureus*	0.9376	0.21	3.35	0.9995	723.61	0.59
	Light					
ZnONPs	0.9641	0.07	9.17	0.9984	822.99	0.57
ZnONPS/*E. coli*	0.683	0.054	12.72	0.9946	560.77	0.79
ZnONPs/*S. aureus*	0.7268	0.063	11.01	0.9947	498.07	0.88

By comparing the correlation coefficient, it is shown that the R^2 of the second-order kinetic model (0.999 and 0.996) is higher than that of the first-order kinetic model (0.955 and 0.791) whether in darkness or light (**Table 5**). Also, values of removal capacities at equilibrium Qe calculated from the second-order model plots (2.273 and 2.21 µg/g) are in good agreement with the experimental values (2.267 and 2.209 µg/g) in both dark and light. Both results suggest that the pseudo second-order mechanism is the predominant process, and the chemisorption mechanism controls the reaction.

The pseudo second rate constant K_2 for ZnONPs/*E. coli*, and ZnONPs/*S. aureus* are 673 and 529 g/mmol min for dark and light (**Table 5**). The half-life times ($t^{1/2} = 1/Q_e K_2$) of the removal are 0.64 and 0.84 min for dark and visible, which showed that the removal of TB dye is faster in the dark. And it is worth mentioning that ZnONPs is much faster and has a higher reaction rate in the light (K_2 = 823 g/mmol min, $t^{1/2}$ = 0.57 min) than in the dark (K_2= 434 g/mmol.min, $t^{1/2}$ = 1.08 min) which may be due to its characteristic photodegradation ability. The overall results showed the removal of TB dye using ZnONPs/*E. coli*, and ZnONPs/*S. aureus* are more appropriate in the darkness while using ZnO is more perfect in the light.

The sorption mechanism of TB dye onto ZnONPs, ZnONPs/*E. coli*, and ZnONPs/*S. aureus* were investigated using Weber-Morris (11), Bangham (12) and Reichenberg (13, 14) equations:

$$Q_t = K_i\sqrt{t} \quad (11)$$

$$\log\log C_0/\left(C_0 - Q_t m\right) = \log K_0 m/2.303V + \propto \log t \quad (12)$$

$$Bt = -0.4977 - \ln(1 - F) \quad (13)$$

$$F = (6/R)(D_i\, t/\pi)^{1/2} \quad (14)$$

where k_i (mmol/g $min^{1/2}$) is the intraparticle diffusion rate coefficient, α and k_0 are constants, the Bt value is a mathematical function of $F = Q_t/Q_e$ and D_i is the effective diffusion coefficient.

Table 6. Comparison of diffusion models parameters for removing TB dye under dark/light conditions.

Sorbent	**Weber- Morris**		**Bangham**		**Reichenberg**	
	ki × 10^{-4} (mmol/g $min^{1/2}$)	R^2	α	R^2	**Di × 10^{-8} (cm^2/ min)**	R^2
Dark						
ZnONPs	0.8	0.953	0.057	0.956	1.7	0.936
ZnONPS/*E. coli*	1.1	0.966	0.078	0.973	3.8	0.968
ZnONPs/*S. aureus*	1	0.944	0.071	0.973	3.7	0.938
Light						
ZnONPs	0.75	0.949	0.066	0.876	1.77	0.804
ZnONPs/*E. coli*	0.89	0.940	0.067	0.859	2.08	0.858
ZnONPs/*S. aureus*	0.88	0.967	0.074	0.936	2.09	0.947

A plot of Q_t versus $t^{1/2}$ gives a straight line with average R^2 values of 0.954 and 0.952 in dark and light (**Table 6**). The straight line did not pass through the origin and the zero intercept (0.0017) indicates the small boundary layer effect. The average values of diffusion rates k_i for darkness and light are 9.7 and 8.4×10^{-5} mmol/g $min^{1/2}$.

The double logarithmic of Bangham equation was plotted against log (t) yielding a perfect linear plot. The average R^2 values are 0.967 and 0.89 and α values (α <1) are 0.069 and 0.0705 for dark and light (**Table 6**). The result shows that the diffusion of TB dye onto the pores of ZnONPs, ZnONPs/*E. coli*, and ZnONPs/*S. aureus* may be involved in the rate controlling step.

The relation between Bt against t was estimated with average R^2 values of 0.947 and 0.87 in the dark and light (**Table 6**). The linearity of this plot can be used to indicate that a partial film is formed along with intraparticle diffusion. The slope of the linear plot of F against $t^{1/2}$ gives the value of the effective diffusion coefficient (Di). The average values of Di are 3.07×10^{-8} and 1.98×10^{-8} cm^2/ min for dark and light indicating that the film diffusion is also involved in the rate-determined step.

By comparing our study with other research, TB was completely removed (98%–100%) using ZnONPs/*E. coli*, and ZnONPs/*S. aureus* within 25–30 min; over a wide pH range (5–9); whether in the dark or light. Pinontoan et al.; demonstrated that Trypan blue dye decolorization by isolated *Aeromonas caviae* was achieved with 77.10% at pH 7.0, and 27 ℃, over six days [40]. Also, Eddy et al.; evaluated mesoporous adsorbent for TB dye removal with an efficiency of 97.10% [41]. In addition, Andrew et al.; optimized the ideal conditions for TB degradation using copper sulfide nanoparticles as pH 10.91, 77.46 min, and 4.999 g/L [42]. Hegde et al.; designed a new composite for the adsorption of TB from wastewater with an excellent 98% removal efficiency, within 10 min of contact time [43].

3.3. Applications

The removal of TB dye of real wastewater samples using ZnONPs, ZnONPs/*E. coli*, and ZnONPs/*S. aureus* was applied. Four different samples from Damietta, Egypt, including, Nile wastewater, industrial wastewater, Lab wastewater and washing wastewater were examined.

Table 7. Removing percentages of TB dye from wastewater.

Sorbents	Nile wastewater		Industrial wastewater		Lab wastewater		Washing wastewater	
	%	RSD%	%	RSD%	%	RSD%	%	RSD%
ZnONPs	87	2.1	86	1.2	90	1.9	84	2.2
ZnONPS/*E. coli*	93	1.9	86	1.2	92	1.4	86	1.4
ZnONPs/*S. aureus*	94	1.9	89	1.2	96	1.2	92	1.2

The average removal rates of TB dye using ZnONPs/*E. coli*, and ZnONPs/*S. aureus* were in the range of 86%–96%, which is more efficient than ZnONPs (84%–90%). The average value of RSD% was 1.7% (and $n = 5$), which is considered as an acceptable value (less than 10%) for real samples (**Table 7**). The results showed a good accuracy of the modified ZnONPs/*E. coli*, and ZnONPs/*S. aureus* in the removal of TB dye from real samples.

4. Conclusion

A new biosorbent was developed by collecting *E. coli* and *S. aureus* bacterial proteins and coating it onto ZnONPs surface. Bacterial proteins were successfully immobilized on ZnONPs surfaces as identified by SEM, XRD, BET and Bradford assay. The improvement of the particle size and surface charge of ZnONPs/*E. coli*, and ZnONPs/*S. aureus* resulted in a lower energy gap and higher conductivity. The modified ZnONPs/*E. coli*, and ZnONPs/*S. aureus* showed significant efficiency in removal of TB dye over a wide pH range (5–9). The removal process was spontaneous, endothermic in dark and exothermic in light. The kinetic studies were followed by pseudo second-order model in the dark/visible indicating a chemisorption removal. The equilibrium isotherms showed that the Freundlich equation has a good fit to the experimental data in the visible while Langmuir model has a good correlation coefficient in the dark. Mechanism of adsorption process was also interpreted with the help of diffusion models and the results exhibited the influence of intraparticle, film and pore diffusion models in the overall removal process. This research can be applied by collecting the found bacteria in wastewater and replacing it with a useful biosorbent for dye removal.

Author contributions: Conceptualization, EAM and TAH; methodology, MSE, EAM and TAH; software, MSE; validation, MSE, EAM and TAH; formal analysis, MSE; investigation, MSE; resources, MSE; data curation, MSE; writing—original draft preparation, MSE; writing—review and editing, MSE; visualization, MSE; supervision, EAM; project administration, EAM; funding acquisition, TAH. All authors have read and agreed to the published version of the manuscript.

Conflict of interest: The authors declare no conflict of interest.

References

1. Czekała W, Pulka J. Water, Wastewater, Waste Management in Agriculture and Agri-Food Industry. Water. 2024; 16(13): 1817. doi: 10.3390/w16131817
2. Mohamed Noor MH, Ngadi N. Global research landscape on coagulation-flocculation for wastewater treatment: A 2000–2023 bibliometric analysis. Journal of Water Process Engineering. 2024; 64: 105696. doi: 10.1016/j.jwpe.2024.105696
3. Amini M, Ashrafi M. Photocatalytic degradation of some organic dyes under solar light irradiation using TiO2 and ZnO nanoparticles. Nanochemistry Research; 2016.
4. Ngulube KF, Abdelhaleem A, Osman AI, et al. Advancing sustainable water treatment strategies: harnessing magnetite-based photocatalysts and techno-economic analysis for enhanced wastewater management in the context of SDGs. Environmental Science and Pollution Research; 2024.
5. Pathania D, Sharma S, Singh P. Removal of methylene blue by adsorption onto activated carbon developed from Ficus carica bast. Arabian Journal of Chemistry. 2017; 10: S1445-S1451. doi: 10.1016/j.arabjc.2013.04.021
6. Erkurt HA, Olaifa JT. Biosorption of Levafix brilliant blue dye using dried Saccharomyces cerevisiae: kinetics, equilibrium, and thermodynamic assessment. Desalination and Water Treatment. 2021; 233: 377-386. doi: 10.5004/dwt.2021.27536
7. Padhi B. Pollution due to synthetic dyes toxicity & carcinogenicity studies and remediation. International Journal of Environmental Sciences. 2012.
8. Lalnunhlimi S, Krishnaswamy V. Decolorization of azo dyes (Direct Blue 151 and Direct Red 31) by moderately alkaliphilic bacterial consortium. Brazilian Journal of Microbiology. 2016; 47(1): 39-46. doi: 10.1016/j.bjm.2015.11.013
9. Moawed EA, El-Shahat MF. Equilibrium, kinetic and thermodynamic studies of the removal of triphenyl methane dyes from wastewater using iodopolyurethane powder. Journal of Taibah University for Science. 2016; 10(1): 46-55. doi: 10.1016/j.jtusci.2015.03.008
10. Pandey A, Singh P, Iyengar L. Bacterial decolorization and degradation of azo dyes. International Biodeterioration & Biodegradation. 2007; 59(2): 73-84. doi: 10.1016/j.ibiod.2006.08.006
11. Josephy PD, Allen-Vercoe E. Reductive metabolism of azo dyes and drugs: Toxicological implications. Food and Chemical Toxicology. 2023; 178: 113932. doi: 10.1016/j.fct.2023.113932
12. Leelakriangsak M. Molecular approaches for bacterial azoreductases. Songklanakarin Journal of Science & Technology. 2013.
13. Rao ANS, Venkatarangaiah VT. Electrochemical treatment of trypan blue synthetic wastewater and its degradation pathway. Journal of Electrochemical Science and Engineering. 2013.
14. Busi S, Chatterjee R, Rajkumari J, Hnamte S. Ecofriendly biosorption of dyes and metals by bacterial biomass of Aeromonas hydrophila RC1. Journal of Environmental Biology. 2016.
15. Omoyeni TM, Erkurt H, Olaifa JT. Biosorption of Dimethyl Phthalate from Aqueous Solution Using Yeast-Based Silver Nanoparticle. Water, Air, & Soil Pollution. 2024; 235(2). doi: 10.1007/s11270-024-06942-8
16. Javanbakht V, Alavi SA, Zilouei H. Mechanisms of heavy metal removal using microorganisms as biosorbent. Water Science and Technology. 2013; 69(9): 1775-1787. doi: 10.2166/wst.2013.718
17. Giese EC, Silva DDV, Costa AFM, et al. Immobilized microbial nanoparticles for biosorption. Critical Reviews in Biotechnology. 2020; 40(5): 653-666. doi: 10.1080/07388551.2020.1751583
18. Banerjee S, Dubey S, Gautam RK, et al. Adsorption characteristics of alumina nanoparticles for the removal of hazardous dye, Orange G from aqueous solutions. Arabian Journal of Chemistry. 2019; 12(8): 5339-5354. doi: 10.1016/j.arabjc.2016.12.016
19. Akpomie KG, Conradie J. Enhanced surface properties, hydrophobicity, and sorption behavior of ZnO nanoparticle–impregnated biomass support for oil spill treatment. Environmental Science and Pollution Research. 2021; 28(20): 25283-25299. doi: 10.1007/s11356-021-12451-6
20. Vaseem M, Umar A, Hahn YB. ZnO nanoparticles: growth, properties, and applications. In: Metal Oxide Nanostructures and Their Applications. New York: American Scientific Publishers; 2010.
21. Navale GR, Thripuranthaka M, Late DJ, Shinde SS. Antimicrobial activity of ZnO nanoparticles against pathogenic bacteria and fungi. JSM Nanotechnol Nanomed; 2015.
22. Martins SCS, Martins CM, Fiúza LMCG, Santaella ST. Immobilization of microbial cells: A promising tool for treatment of toxic pollutants in industrial wastewater. African journal of biotechnology. 2013; 12(28).

23. Louie SM, Pettibone JM. Research highlights: probing adsorbed organic coatings on nanoparticle surfaces. Environmental Science: Nano. 2015; 2(5): 417-420. doi: 10.1039/c5en90019k
24. Shao Q, Hall CK. Protein adsorption on nanoparticles: model development using computer simulation. Journal of Physics: Condensed Matter. 2016; 28(41): 414019. doi: 10.1088/0953-8984/28/41/414019
25. Rabe M, Verdes D, Seeger S. Understanding protein adsorption phenomena at solid surfaces. Advances in Colloid and Interface Science. 2011; 162(1-2): 87-106. doi: 10.1016/j.cis.2010.12.007
26. Gray JJ. The interaction of proteins with solid surfaces. Current Opinion in Structural Biology. 2004; 14(1): 110-115. doi: 10.1016/j.sbi.2003.12.001
27. Cao Z, Zhang Z, Wang F, et al. Synthesis and UV shielding properties of zinc oxide ultrafine particles modified with silica and trimethyl siloxane. Colloids and Surfaces A: Physicochemical and Engineering Aspects. 2009; 340(1-3): 161-167. doi: 10.1016/j.colsurfa.2009.03.024
28. Jacobsson TJ. Synthesis and characterisation of ZnO nanoparticles. An experimental investigation of some of their size dependent quantum effects. 2010.
29. Hamedani NF, Farzaneh F. Synthesis of ZnO nanocrystals with hexagonal (Wurtzite) structure in water using microwave irradiation. Journal of Sciences, Islamic Republic of Iran. 2006.
30. Xiong G, Pal U, Serrano JG, et al. Photoluminesence and FTIR study of ZnO nanoparticles: the impurity and defect perspective. Physica Status Solidi C. 2006; 3(10): 3577-3581. doi: 10.1002/pssc.200672164
31. Alwan RM, Kadhim QA, Sahan KM, et al. Synthesis of zinc oxide nanoparticles via sol-gel route and their characterization. Nanoscience and Nanotechnology; 2015
32. Hedayati K. Fabrication and Optical Characterization of Zinc Oxide Nanoparticles Prepared via a Simple Sol-gel Method. Journal of Nanostructures. 2015.
33. Kulkarni S S, Shirsat M D (2015). Optical and structural properties of zinc oxide nanoparticles. International Journal of Advanced Research in Physical Science, 2(1): 14-18
34. Moghri Moazzen MA, Borghei SM, Taleshi F. Change in the morphology of ZnO nanoparticles upon changing the reactant concentration. Applied Nanoscience. 2012; 3(4): 295-302. doi: 10.1007/s13204-012-0147-z
35. Talam S, Karumuri SR, Gunnam N. Synthesis, Characterization, and Spectroscopic Properties of ZnO Nanoparticles. ISRN Nanotechnology. 2012; 2012: 1-6. doi: 10.5402/2012/372505
36. Bradford MM. A rapid and sensitive method for the quantitation of microgram quantities of protein utilizing the principle of protein-dye binding. Analytical biochemistry; 1976.
37. McGuffie MJ, Hong J, Bahng JH, et al. Zinc oxide nanoparticle suspensions and layer-by-layer coatings inhibit staphylococcal growth. Nanomedicine: Nanotechnology, Biology and Medicine. 2016; 12(1): 33-42. doi: 10.1016/j.nano.2015.10.002
38. Gao H, Zhao J. Interaction of Trypan Blue with Protein and Application. Journal of the Chinese Chemical Society. 2003; 50(2): 329-334. doi: 10.1002/jccs.200300049
39. Aljeboree AM, Alshirifi AN, Alkaim AF. Kinetics and equilibrium study for the adsorption of textile dyes on coconut shell activated carbon. Arabian Journal of Chemistry. 2017; 10: S3381-S3393. doi: 10.1016/j.arabjc.2014.01.020
40. Pinontoan R, Susanto Tsr, Lucy J, et al. Trypan blue dye decolorization by Aeromonas caviae isolated from water sewage in Jakarta, Indonesia. Biodiversitas Journal of Biological Diversity. 2024; 25(4). doi: 10.13057/biodiv/d250432
41. Eddy NO, Garg R, Garg R, et al. Waste to resource recovery: mesoporous adsorbent from orange peel for the removal of trypan blue dye from aqueous solution. Biomass Conversion and Biorefinery. 2022; 13(15): 13493-13511. doi: 10.1007/s13399-022-02571-5
42. Andrew FP, Papo TR, Ajibade PA. Optimization of trypan blue and brilliant green dyes photocatalytic degradation and adsorption of lead (II) and chromium (VI) heavy metal ions by copper sulfide nanoparticles. Environmental Advances. 2024; 17: 100575. doi: 10.1016/j.envadv.2024.100575
43. Hegde V, Uthappa UT, Suneetha M, et al. Functional porous Ce-UiO-66 MOF@Keratin composites for the efficient adsorption of trypan blue dye from wastewater: A step towards practical implementations. Chemical Engineering Journal. 2023; 461: 142103. doi: 10.1016/j.cej.2023.142103